

# 光学学报

## 三维显微测振中离轴光路机械形变对耦合效率的影响

董辉<sup>1</sup>, 王大勇<sup>2</sup>, 孔新新<sup>3</sup>, 王云新<sup>2\*</sup>

<sup>1</sup>北京工业大学材料与制造学部, 北京 100124;

<sup>2</sup>北京工业大学理学部, 北京 100124;

<sup>3</sup>中国科学院计算光学成像技术重点实验室, 北京 100094

**摘要** 三维显微测振仪可用于测量微结构的三维振动, 其两条离轴光路用于接收包含面内振动信息的信号光, 系统的机械形变会直接影响光纤的耦合效率, 从而影响系统的测振精度。结合衍射传播理论和光纤耦合原理, 建立了离轴光路的信号光传输耦合模型, 针对信号光平面与光纤平面存在倾角的问题, 利用频域坐标旋转变换法将倾斜的物面信号光场投影到平行的参考平面上, 再基于菲涅耳衍射传播计算得到光纤平面的光场分布, 进而结合光纤的模场分布可计算得到光纤耦合效率。研究了耦合透镜、光纤等元件的机械形变对光纤耦合效率的影响, 阐明了光纤耦合效率和各个机械变形量的关系, 为三维激光多普勒显微测振系统的设计和装调工作提供了理论指导。

**关键词** 测量; 干涉测量; 三维显微测振; 机械形变; 光纤耦合; 衍射传播理论

中图分类号 O436

文献标志码 A

DOI: 10.3788/AOS221963

### 1 引言

近年来激光多普勒测振技术<sup>[1-2]</sup>在农业、生命医学、航空航天和建筑工程领域中有着广泛的应用<sup>[3-4]</sup>。三维激光多普勒显微测振<sup>[5]</sup>作为一种新型的激光多普勒测量技术, 凭借空间分辨率高、能够获取三维振动信息和测振精度高等特点, 被广泛应用于微结构物体的动态特性研究中。这项技术不仅可以得到微结构物体的面外振动信息, 还可以得到其面内振动信息, 这是因为相较于一维激光多普勒测振系统, 该技术增加了两条离轴光路, 分别用来接收微结构物体在面内  $x$  方向和  $y$  方向的振动信息。三维显微测振仪中离轴信号接收光路的外差探测效率主要决定于光纤耦合效率, 其决定了进入光电探测器的能量, 会直接影响系统的测振精度。为了防止损坏样品, 高精度的测振系统对出射的信号光功率有所限制, 进而需要保证系统的光纤耦合效率。影响测振系统中光纤耦合效率的因素有很多, 如光学系统的像差会引起发射和接收光场产生波前畸变, 从而影响外差效率。李成强<sup>[6]</sup>研究了光学系统的像差对一维光通信激光外差探测性能的影响, 给出了各种初级像差对外差效率影响所占的权重。对于用于长距离探测的激光外差系统, 必须要考虑大气湍流的影响, 大气湍流会使经过其中的光束波前发生畸

变, 从而影响探测系统的性能。南友新<sup>[7]</sup>研究了大气湍流对一维外差探测系统空间光-光纤耦合效率的影响, 在 Kolmogorov 湍流谱模型下, 分析了光源相干度、光源波长、湍流强度和传输距离等因素对耦合效率的影响。赵中华等<sup>[8]</sup>探究了平面光、高斯光和艾里光作为信号光时, 信号光与参考光的相干外差效率随耦合透镜  $F$  数、束腰半径和光敏面面积等参数的变化, 为一维激光多普勒探测系统信号光耦合系统提供了参数优化方案。王骐等<sup>[9]</sup>分析了星间相干光通信系统中本振光和信号光振幅分布类型、光束自身参数、探测器光敏面半径大小和聚焦系统参数对系统外差效率的影响。Rembe 等<sup>[5]</sup>对三维显微测振仪的主轴镜头和离轴耦合透镜的参数选定进行了研究, 确定了主轴镜头工作距、数值孔径和离轴耦合透镜数值孔径等参数的设计要求, 为三维显微测振仪前端信号光耦合系统的设计提供了参考。

目前的研究主要存在两方面不足。一方面, 大部分研究都是针对一维激光多普勒探测系统, 缺乏对激光多普勒三维显微测振系统的研究, 尤其是离轴信号接收光路的研究。另一方面, 系统装调也存在一定的误差, 并且系统实际使用过程中, 重力、温度等因素均会引起系统发生机械形变, 这些因素对光纤耦合效率的影响不可忽略, 但这一方面的研究仍然较少。针对

收稿日期: 2022-11-10; 修回日期: 2022-12-18; 录用日期: 2022-12-30; 网络首发日期: 2023-01-06

基金项目: 国家自然科学基金(62075001, 62275008)

通信作者: \*yxwang@bjut.edu.cn

上述问题,基于衍射传播理论和光纤耦合原理,建立了三维显微测振系统中离轴信号接收光路的光传输和耦合模型。针对系统中主要的机械变形量进行分析,研究了这些变形量对光纤耦合效率的影响,并给出了不同机械变形量的最大容差。该研究对三维激光多普勒显微测振系统的设计和装调工作具有重要意义。

## 2 基本原理

### 2.1 三维显微测振系统光路原理

三维显微测振系统的探测光路包括主轴光路和离轴光路。主轴光路的作用是将激光入射至待测物体,并接收包含物体 $z$ 方向振动分量信息的反射信号光,两条离轴光路的作用是接收包含物体 $x$ 方向和 $y$ 方向振动分量信息的反射信号光。

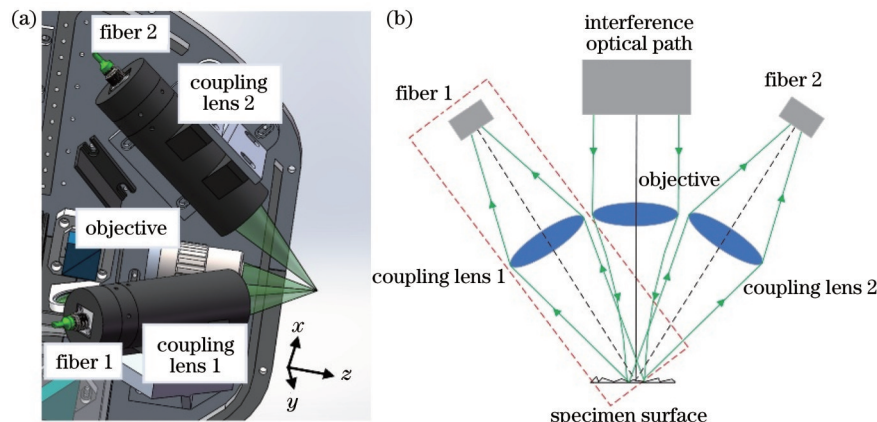


图1 三维激光多普勒显微测振系统探测光路和离轴信号光传输示意图。(a)三维激光多普勒显微测振系统探测光路示意图;(b)离轴信号光传输示意图

Fig. 1 Schematic diagram of detection optical path of three-dimensional laser Doppler micro-vibration measurement system and off-axis signal light transmission. (a) Schematic diagram of detection optical path of three-dimensional laser Doppler micro-vibration measurement system; (b) schematic diagram of off-axis signal light transmission

### 2.2 光场传输算法

从图1(b)可以看出,初始物面光场与离轴耦合透镜前表面是相互倾斜的,故需要考虑两个倾斜面之间的衍射传播过程。因此,建立了离轴信号光传输模型,如图2所示,其中参考物面与透镜平面互相平行。首先,利用频域坐标旋转变换法将物面信号光场投影到参考物面上,获得参考物面的光场分布,完成倾斜校正。然后,光场经过衍射传播距离 $d_0$ 到耦合透镜表面上,经过耦合透镜的相位调制作用,通过衍射传播距离 $d$ 到光纤端面,最终可获得光纤端面上的光场分布。

激光器发出的光波为基模高斯光束,经过显微测振系统前端物镜聚焦在待测物体上,通常可形成微米级的光斑。高斯光束经过光学系统变换后仍为高斯光束,为了达到较高的空间分辨率,聚焦在物面的光场一般会设计在束腰处。设原物面光场 $U_0(x_0, y_0)$ 的坐标向量为 $\mathbf{u} = (x_0, y_0, z_0)$ ,则物面信号光的光场分布可以表示为

三维激光多普勒显微测振系统探测光路如图1(a)所示,其中物镜所在的光路为三维显微测振仪的主轴光路,其与 $z$ 轴重合。另外两条光路为三维显微测振仪的离轴光路,两条离轴光路分别在 $y-z$ 平面和 $x-z$ 平面上,且与主轴光路夹角相同。由于两条离轴光路的衍射传播过程一致,因此只对图1(b)中左侧虚线矩形框标识的离轴光路进行仿真分析。信号光通过主轴的物镜出射,可聚焦成微米级的光斑并照明物体,经物体反射后反射光被离轴光路中的耦合透镜聚焦并耦合进入光纤中,再经过光纤进入干涉光路中进行外差探测。主要研究了离轴信号光传输过程中,因光纤和耦合透镜的机械误差导致的位置或角度偏移对离轴信号光耦合效率的影响。

$$U_0(x_0, y_0, 0) = C_0 \exp\left[-\frac{(x_0 + y_0)^2}{\omega_0^2}\right], \quad (1)$$

式中: $C_0$ 为常数; $\omega_0$ 为物面上高斯光束的束腰半径。忽略待测物体表面的粗糙度影响,只考虑光束方向改变,则对于离轴光路,原物面光场分布可用式(1)表示。

原物面光场的频谱可以由二维傅里叶变换计算得到,即

$$A(f_x, f_y) = \mathcal{F}[U_0(x_0, y_0)] = \iint U_0(x_0, y_0) \times \exp[-j2\pi(f_x x_0 + f_y y_0)] dx_0 dy_0, \quad (2)$$

式中: $\mathcal{F}(\cdot)$ 为傅里叶变换函数; $(f_x, f_y, f_z)$ 为原物面空间频率坐标,其中 $f_z^2 = (1 - f_x^2 - f_y^2)/\lambda$ , $\lambda$ 为波长。设物平面绕 $y$ 轴旋转角度 $\theta$ 后可获得与耦合透镜平面平行的参考物面,参考面的坐标向量用 $\mathbf{u}' = (x', y', z')$ 表示,对应的空间频率坐标可以表示为 $(f_{x'}, f_{y'}, f_{z'})$ ,其中 $f_{z'}^2 = (1 - f_{x'}^2 - f_{y'}^2)/\lambda$ 。将原物面旋转投影到参考物面

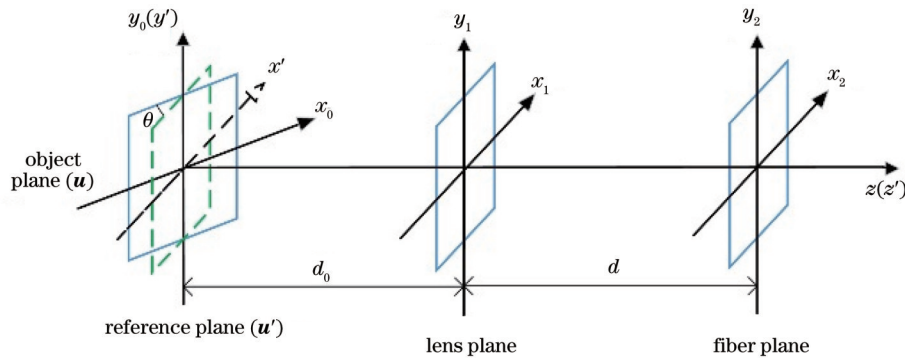


图2 离轴信号光传播示意图

Fig. 2 Schematic diagram of off-axis signal light propagation

上,两平面的频率坐标满足的对应关系<sup>[10]</sup>为

$$\begin{bmatrix} f_x \\ f_y \\ f_z \end{bmatrix} = \begin{bmatrix} \cos \theta & 0 & \sin \theta \\ 0 & 1 & 0 \\ -\sin \theta & 0 & \cos \theta \end{bmatrix} \begin{bmatrix} f_{x'} \\ f_{y'} \\ f_{z'} \end{bmatrix}, \quad (3)$$

展开可以得出

$$\begin{cases} f_x = \alpha(f_{x'}, f_{y'}) = f_{x'} \cos \theta + \frac{1 - f_{x'}^2 - f_{y'}^2}{\lambda} \sin \theta, \\ f_y = \beta(f_{x'}, f_{y'}) = f_{y'} \end{cases}, \quad (4)$$

故参考物面的频谱可以表示为

$$G(f_{x'}, f_{y'}) = A[\alpha(f_{x'}, f_{y'}), \beta(f_{x'}, f_{y'})]. \quad (5)$$

根据能量守恒定律,积分面元还需满足

$$df_x df_y = |J(f_{x'}, f_{y'})| df_{x'} df_{y'}, \quad (6)$$

式中: $J(\cdot)$ 为雅克比行列式<sup>[11]</sup>,可以表示为

$$|J(f_{x'}, f_{y'})| = \left| \begin{bmatrix} \frac{\partial \alpha}{\partial f_{x'}} & \frac{\partial \alpha}{\partial f_{y'}} \\ \frac{\partial \beta}{\partial f_{x'}} & \frac{\partial \beta}{\partial f_{y'}} \end{bmatrix} \right| = \cos \theta + \frac{f_{x'}}{f_{z'}} \sin \theta. \quad (7)$$

参考物面光场可由对参考物面频谱进行傅里叶逆变换得到,即

$$\begin{aligned} U_r(x', y') &= \mathcal{F}^{-1}[G(f_{x'}, f_{y'})] = \\ &\iint A[\alpha(f_{x'}, f_{y'}), \beta(f_{x'}, f_{y'})] \times \\ &\exp[j2\pi(f_{x'}x' + f_{y'}y')] |J(f_{x'}, f_{y'})| df_{x'} df_{y'}, \end{aligned} \quad (8)$$

式中: $\mathcal{F}^{-1}(\cdot)$ 为傅里叶逆变换函数。将式(4)和式(7)代入式(8)中可得

$$\begin{aligned} U_r(x', y') &= \iint G\left(f_{x'} \cos \theta + \frac{1 - f_{x'}^2 - f_{y'}^2}{\lambda} \sin \theta, f_{y'}\right) \times \\ &\exp[j2\pi(f_{x'}x' + f_{y'}y')] \left| \cos \theta + \frac{f_{x'}}{f_{z'}} \sin \theta \right| df_{x'} df_{y'}. \end{aligned} \quad (9)$$

为了方便后续分析误差,基于菲涅耳衍射传播<sup>[12]</sup>进行光场传输的计算。在傍轴条件下,耦合透镜前表面光场可以表示为

$$U(x_1, y_1) = \frac{\exp(jkd_0)}{j\lambda d_0} \iint U_r(x', y') \times \exp\left\{\frac{jk}{2d_0} [(x_1 - x')^2 + (y_1 - y')^2]\right\} dx' dy', \quad (10)$$

式中: $k = 2\pi/\lambda$ 为波数。

同理,光纤端面处的光场可以表示为

$$U_i(x_2, y_2) = \frac{\exp(jkd)}{j\lambda d} \iint U(x_1, y_1) \tilde{t}(x_1, y_1) \times \exp\left\{\frac{jk}{2d} [(x_2 - x_1)^2 + (y_2 - y_1)^2]\right\} dx_1 dy_1, \quad (11)$$

式中: $\tilde{t}(x_1, y_1)$ 为耦合透镜的相位调制因子,可以表示为

$$\tilde{t}(x_1, y_1) = P(x_1, y_1) \exp\left[-j\frac{k}{2f}(x_1^2 + y_1^2)\right], \quad (12)$$

式中: $P(x_1, y_1)$ 为透镜的孔径函数。

接着,采用模场匹配法分析离轴信号光耦合效率,耦合效率<sup>[13]</sup>可以表示为

$$\eta = \frac{\left| \iint_{S_1} U_i(x_2, y_2) U_f^*(x_2, y_2) dx_2 dy_2 \right|^2}{\iint_{S_2} |U_i(x_2, y_2)|^2 dx_2 dy_2 \iint_{S_2} |U_f(x_2, y_2)|^2 dx_2 dy_2}, \quad (13)$$

式中: $U_f(x_2, y_2)$ 为光纤模场分布; $U_f^*(x_2, y_2)$ 为 $U_f(x_2, y_2)$ 的复共轭; $S_1$ 为两个光场的交叠面积; $S_2$ 为光纤端面的面积。可以看出,两束光波模场的振幅和相位越接近,耦合效率越高。由于单模光纤只能传输基模,故基模在光纤端面上的模场分布<sup>[13]</sup>可以用高斯函数表示为

$$U_f(x_2, y_2) = \frac{2}{\pi} \cdot \frac{1}{w_0} \exp\left[-(x_2^2 + y_2^2)/w_0^2\right], \quad (14)$$

式中: $w_0$ 为单模光纤模场半径。

### 3 仿真分析

设所用激光波长为532 nm,离轴光路和主路夹角为40°。原物面光场为高斯分布,无附加相位,束腰半

径为 $2.3\mu\text{m}$ 。原物面到离轴耦合透镜前表面的距离为 $100\text{ mm}$ , 离轴耦合透镜到光纤端面的距离为 $100\text{ mm}$ , 离轴耦合透镜焦距 $f$ 为 $50\text{ mm}$ 、口径 $D$ 为 $20\text{ mm}$ , 单模光纤模场半径为 $2.3\mu\text{m}$ 。在不考虑任何机械形变并忽略物体表面粗糙度影响的情况下, 各个平面的光场分布如图3所示。图3(a)、(b)为原物面光场的振幅和相位分布, 经过旋转变换投影到参考物面上的光场振幅和相位分布如图3(c)、(d)所示。可以看出, 参考物面光场的振幅和相位分布为椭圆形且具

有不对称性, 这一点从相位图像上很容易看出。参考物面上的光场经过衍射传播和耦合镜作用后在光纤端面上的光场振幅和相位分布如图3(e)、(f)所示。由于理想模型中参考物面和光纤端面满足成像关系, 因此光纤端面上的光场相当于参考物面光场等大倒立的实像。同时, 耦合镜的衍射受限也会对最终的结果产生一定的影响。最终, 对光纤端面上的光场与单模光纤模场分布进行模场匹配, 计算得出理想情况下的光纤耦合效率为 $76.5\%$ 。

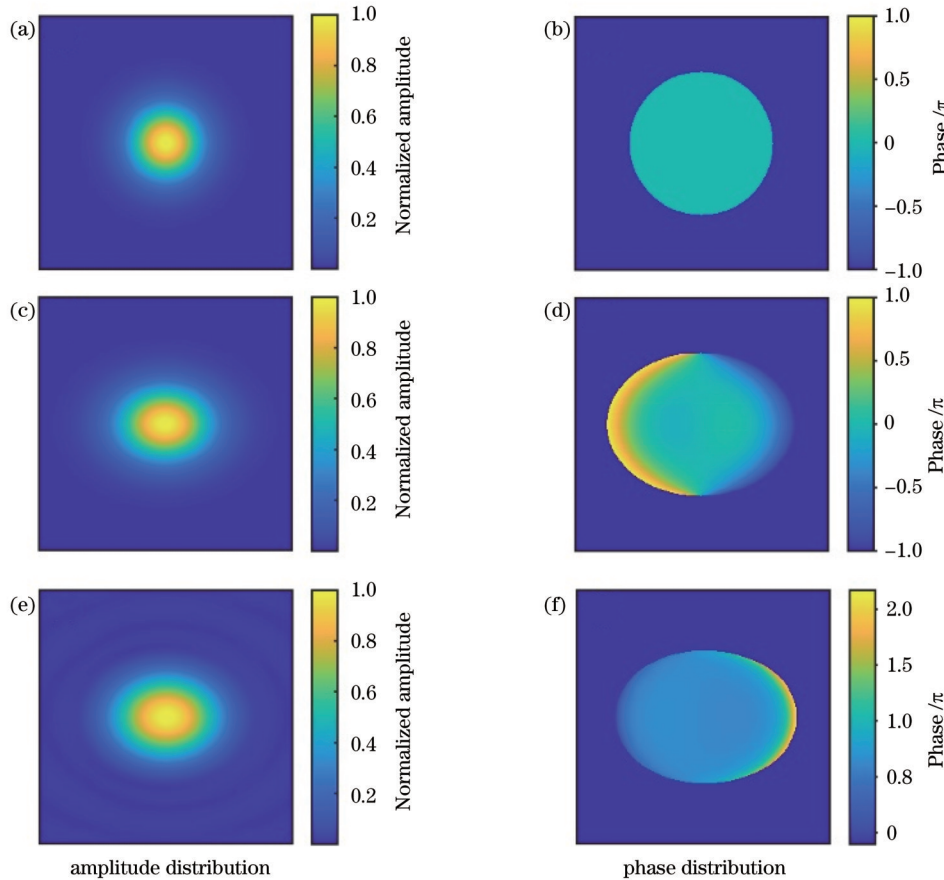


图3 不考虑机械形变影响情况下各平面上的光场分布。(a)(b)原物面;(c)(d)参考物面;(e)(f)光纤端面

Fig. 3 Light field distribution on each plane without mechanical deformation. (a)(b) Original plane; (c)(d) reference plane; (e)(f) fiber plane

### 3.1 耦合透镜偏心

首先, 分析耦合透镜偏心对光纤耦合效率的影响。在忽略耦合透镜像差影响的情况下, 耦合透镜对入射光场的相位调制可由式(12)表示。假设耦合透镜在 $x$ 方向产生了 $\Delta x$ 的偏移, 则耦合透镜的相位变换因子转换为

$$\tilde{i}(x_1 + \Delta x, y_1) = P(x_1 + \Delta x, y_1) \times \exp \left\{ -j \frac{k}{2f} [(x_1 + \Delta x)^2 + y_1^2] \right\}, \quad (15)$$

将式(15)代入模型中, 得到耦合透镜偏心量与耦合效率的关系, 仿真结果如图4所示。

通过分析, 透镜偏移会使经过偏移透镜的光场中

心向透镜偏移后新的光轴移动, 而在经过一定的传播距离后, 新的光场中心会与透镜偏移后的光轴重合。由图4可以看出, 当光纤耦合效率优于 $40\%$ 时, 耦合透镜偏心量最大容许范围为 $\pm 1.5\mu\text{m}$ 。

### 3.2 耦合透镜倾斜

倾斜光学元件对光场的作用可以用相位因子<sup>[14]</sup>描述, 即

$$\varphi(x, y) = \exp[-ik(C_1 x + C_2 y)]. \quad (16)$$

假设耦合透镜绕 $x$ 轴有 $\Delta\alpha_1$ 的角度倾斜, 定义倾斜因子为 $C_2 = \tan\Delta\alpha_1$ <sup>[15]</sup>。倾斜耦合透镜如图5所示。

由图5中的几何关系可知, 倾斜相位因子等于光

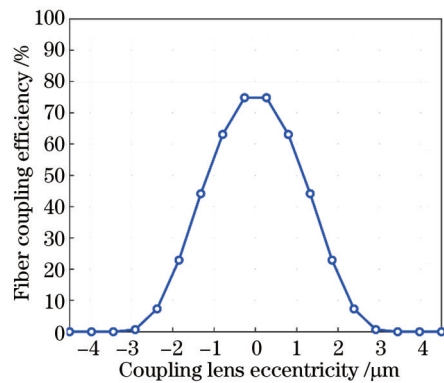


图4 耦合透镜偏心量和光纤耦合效率的关系曲线

Fig. 4 Relationship between coupling lens eccentricity and fiber coupling efficiency

学元件倾斜后形成的楔形空气间隙对原光场的相位调制。经过倾斜透镜后的光场表达式为

$$U'(x_1, y_1) = U(x_1, y_1) \cdot t(x_1, y_1) \cdot \varphi_1(x_1, y_1) \cdot \varphi_2(x_1, y_1), \quad (17)$$

式中: $t(x_1, y_1)$ 为透镜相位变换因子; $\varphi_1(x_1, y_1)$ 为耦合透镜倾斜前端产生的空气间隔导致的相位变换因子; $\varphi_2(x_1, y_1)$ 为耦合透镜倾斜后端产生的空气间隔导致的相位变换因子。由图5的几何关系可得

$$\begin{cases} \varphi_1(x_1, y_1) = \exp(-ik \tan \Delta\alpha_1 y_1) = \exp(-ik C_2 y_1) \\ \varphi_2(x_1, y_1) = \exp[-ik \tan (-\Delta\alpha_1) y_1] = \exp(ik C_2 y_1) \end{cases} \quad (18)$$

由于倾斜耦合透镜前后表面附近因透镜倾斜引起的波前改变相互抵消,故 $\varphi_1(x_1, y_1) \cdot \varphi_2(x_1, y_1) = 1$ 。因此,由以上推导可得,在忽略耦合透镜本身像差的情况下,耦合透镜的倾斜对耦合效率没有影响。

### 3.3 光纤位置错位

光纤端面会因外力等因素发生位置偏移和角度偏移,单模光纤的模场分布可以用式(14)表示。然而,在x方向和y方向有位置偏移 $\Delta x$ 和 $\Delta y$ 的光纤模场分布可以表示为

$$U_f'(x_2, y_2) = \sqrt{\frac{2}{\pi}} \cdot \frac{1}{w_0} \exp \left\{ -[(x_2 + \Delta x)^2 + (y_2 + \Delta y)^2] / w_0^2 \right\}. \quad (19)$$

将式(19)代入耦合效率的积分式中求解计算,即可获得光纤端面在x-y平面的位置偏移与系统耦合效率的关系,仿真结果如图6(a)所示。光纤端面在x方向的位置错位和在y方向的位置错位与耦合效率的关系不同,这是由光在倾斜面间传播,最终光纤模场投影为椭圆形导致的。x方向对应椭圆形光场的长边,y方向对应椭圆形光场的短边。

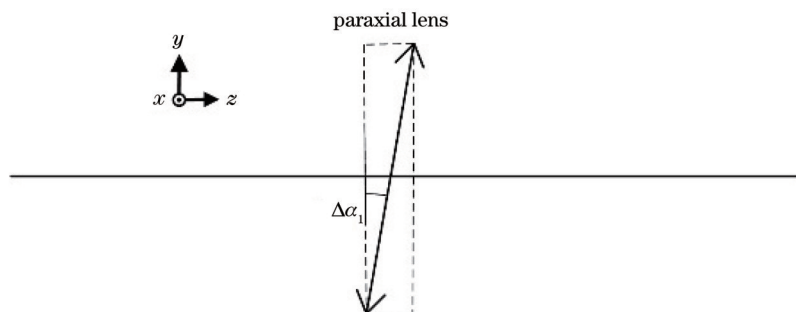


图5 倾斜透镜模型

Fig. 5 Tilt lens model

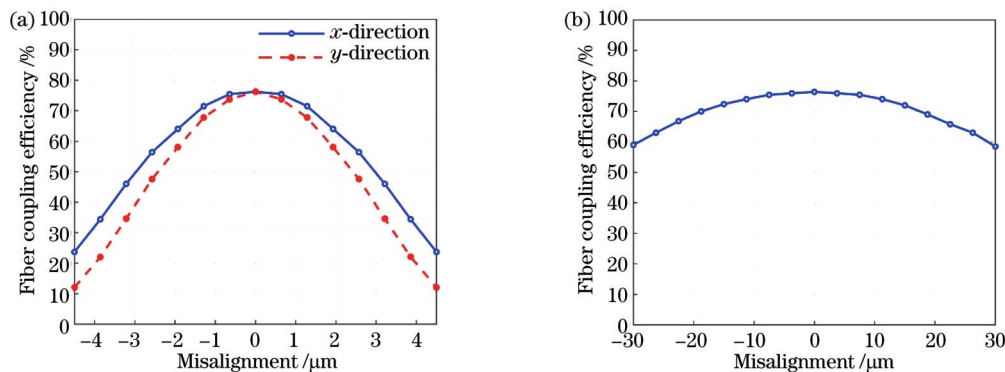


图6 光纤位置错位与耦合效率的关系。(a) x-y平面;(b) z方向

Fig. 6 Relationship between misalignment of optical fiber and coupling efficiency. (a) x-y plane; (b) z direction

光纤端面在 $z$ 轴方向的位置偏移会导致光纤到耦合透镜面衍射距离的变化,引起光场离焦,从而导致耦合效率发生改变。由图6(b)可以看出,在 $z$ 方向的位置偏移容许量较大,这是由高斯光束的特性导致的。在束腰附近的瑞利长度范围内光场变化量很小,而激光的瑞利长度定义为束腰处到束腰半径增加到 $\sqrt{2}$ 倍(在传播方向上)处的距离,计算得到瑞利长度为

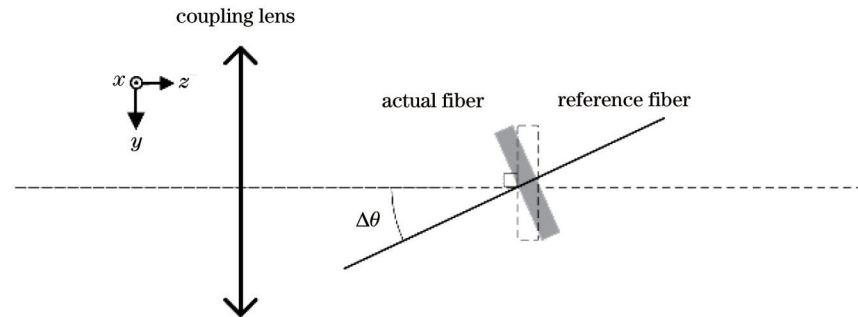


图7 光纤角度错位示意图

Fig. 7 Schematic diagram of fiber angle misalignment

光纤端面的角度偏移会使透镜后表面与光纤端面平面成一定夹角,故需要用2.2节中的频域坐标旋转变换法,将光纤错位角为 $0^\circ$ 时的光纤端面看作理想参考面并将其旋转投影到不同光纤错位角对应的光纤端面上,再将得到的实际光纤端面上的光场与光纤模场耦合,从而得到不同光纤错位角对应的光纤耦合效率。设光纤错位角仅存在于 $y$ - $z$ 平面上,则光纤错位角越大,投影在实际光纤端面上的光场与理想的光纤模场差距越大,从而导致耦合效率随之逐渐下降。

光纤错位角与耦合效率的关系如图8所示。可以看出,当光纤错位角在 $\pm 15^\circ$ 范围内时,耦合效率从76.5%下降到了68.0%左右,说明耦合效率对光纤错位角这一变形量较不敏感。

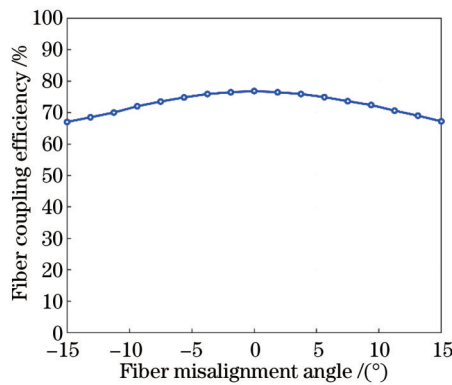


图8 光纤端面的错位角与耦合效率的关系

Fig. 8 Relationship between fiber misalignment angle and coupling efficiency

### 3.5 面外振动

由于待测物体在 $z$ 方向会产生振动,这势必会引起待测物体的离焦和光场偏移,从而导致耦合效率下

降。然而,随着振动幅度的增大,待测物体的离焦程度也会增大,光纤耦合效率也会随之下降。因此,需要测定三维显微测振系统面外振动的测量范围。

### 3.4 光纤角度错位

光纤角度错位也会导致耦合效率损耗,如图7所示,在引入光纤错位角 $\Delta\theta$ 后,光纤端面到耦合透镜表面为倾斜面间的传播,以光纤端面为基准面,耦合透镜表面相对于参考面的倾角也为 $\Delta\theta$ 。

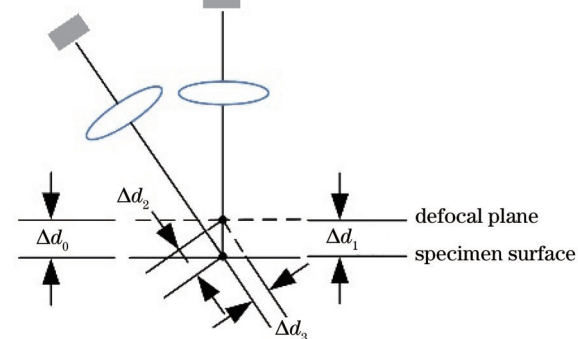


图9 面外振动引起的机械形变量示意图

Fig. 9 Schematic diagram of mechanical form variables caused by out-of-plane vibration

在离轴光场传播坐标系下的初始光场即为参考面上的光场 $U_r(x', y', 0)$ ,而经面外振动引起的位移形

变量影响后的初始光场为  $U_r(x' + \Delta d_3, y', \Delta d_2)$ 。由以上分析可得待测物体面外振动位移与耦合效率的关系,如图10所示。可以看出,当面外振动位移在  $\pm 3 \mu\text{m}$  范围内时,耦合效率从 76.5% 下降到 60.0% 左右,这在系统的实际使用过程中是可以接受的。

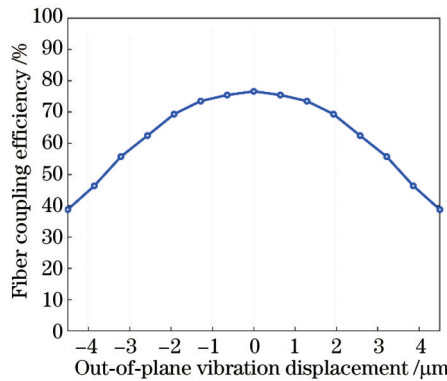


图10 面外振动位移与耦合效率的关系

Fig. 10 Relationship between out-of-plane vibration displacement and coupling efficiency

## 4 结 论

建立了三维激光多普勒显微测振系统中离轴信号光传输与耦合模型,针对模型中存在光传输到倾斜平面上的情况,采用频域坐标变换法对物面光场进行校正,并进行了数值仿真计算,使得得出的结果更符合实际情况。进一步研究了三维激光多普勒显微测振系统中机械变形量对离轴信号光耦合效率的影响。离轴信号光耦合效率对耦合透镜偏心量和光纤的位置错位较为敏感。在微米级位移误差下,离轴耦合效率急剧下降,故在设计系统时应优先避免这两种机械误差。然而,离轴信号光耦合效率对光纤端面的离焦和光纤角度错位较不敏感。在实际系统使用时,若待测物体的面外振动范围为  $\pm 3 \mu\text{m}$ ,此范围内离轴信号光的耦合效率从 76.5% 缓慢下降至 60.0% 左右,对系统影响较小。在忽略耦合透镜本身像差的情况下,耦合透镜倾斜对耦合效率没有影响。本研究对三维激光多普勒显微测振系统离轴探测光路的设计具有重要意义,其衍射传播计算思路和耦合模型的构建与分析思路可进一步推广到其他单模光纤成像系统中。

## 参 考 文 献

- [1] Rembe C, Siegmund G, Steger H, et al. Measuring MEMS in motion by laser Doppler vibrometry[M]//Osten W. Optical inspection of microsystems. 2nd ed. Boston: CRC Press, 2019: 297-347.
- [2] 鹿彤彤, 陆彦婷, 杜福嘉, 等. 瞳面干涉激光多普勒测振[J]. 光学学报, 2022, 42(15): 1512005.
- [3] 张驰, 王顺, 关向雨, 等. 激光多普勒测振技术应用的新进展[J]. 激光与光电子学进展, 2022, 59(19): 1900006.
- [4] Zhang C, Wang S, Guan X Y, et al. New progress in application of laser Doppler vibration measurement technology [J]. Laser & Optoelectronics Progress, 2022, 59(19): 1900006.
- [5] 张志平, 杨晓峰. 激光外差干涉技术在光刻机中的应用[J]. 激光与光电子学进展, 2022, 59(9): 0922017.
- [6] Zhang Z P, Yang X F. Application of laser heterodyne interference technology in lithography[J]. Laser & Optoelectronics Progress, 2022, 59(9): 0922017.
- [7] Rembe C, Kowarsch R, Ochs W, et al. Optical three-dimensional vibrometer microscope with picometer-resolution in  $x$ ,  $y$ , and  $z$ [J]. Optical Engineering, 2014, 53(3): 034108.
- [8] 李成强. 激光外差探测系统性能光学影响因素研究[D]. 长春: 中国科学院长春光学精密机械与物理研究所, 2016.
- [9] Li C Q. Investigating the effect of optics factors on the performance of laser heterodyne detection system[D]. Changchun: Changchun Institute of Optics, Fine Mechanics and Physics, Chinese Academy of Sciences, 2016.
- [10] 南友新. 大气湍流信道中部分相干光-单模光纤耦合效率研究[D]. 西安: 西安理工大学, 2021.
- [11] Nan Y X. Research on coupling efficiency of partially coherent light-single mode fiber in atmospheric turbulence channel[D]. Xi'an: Xi'an University of Technology, 2021.
- [12] 赵中华, 辛海燕. 不同相干光通信外差效率的数值计算与分析[J]. 光通信技术, 2018, 42(4): 59-62.
- [13] Zhao Z H, Xin H Y. Numerical calculation and analysis of heterodyne efficiency for different coherent optical communication[J]. Optical Communication Technology, 2018, 42(4): 59-62.
- [14] 王骐, 王春晖, 尚铁梁. 高斯本振光和爱里斑信号光相干探测的外差效率[J]. 中国激光, 2003, 30(s1): 183-186.
- [15] Wang Q, Wang C H, Shang T L. Heterodyne efficiency of coherent detection with Gaussian local-oscillator and airy spot signal beam[J]. Chinese Journal of Lasers, 2003, 30(s1): 183-186.
- [16] Matsushima K. Formulation of the rotational transformation of wave fields and their application to digital holography[J]. Applied Optics, 2008, 47(19): D110-D116.
- [17] Picart P, Tankam P, Mounier D, et al. Spatial bandwidth extended reconstruction for digital color Fresnel holograms[J]. Optics Express, 2009, 17(11): 9145-9156.
- [18] Goodman J W. 傅里叶光学导论[M]. 陈家璧, 秦克诚, 曹其智, 译. 第四版. 北京: 科学出版社, 2020.
- [19] Goodman J W. Introduction to Fourier optics[M]. Chen J B, Qin K C, Cao Q Z, et al., Transl. 4th ed. Beijing: Science Press, 2020.
- [20] Wagner R E, Tomlinson W J. Coupling efficiency of optics in single-mode fiber components[J]. Applied Optics, 1982, 21(15): 2671-2688.
- [21] Alda J, Alonso J, Bernabeu E. Characterization of aberrated laser beams[J]. Journal of the Optical Society of America A, 1997, 14(10): 2737-2747.
- [22] 赵延伸, 孙华燕, 宋丰华, 等. 倾斜离轴高斯光束通过猫眼光学镜头的传输特性[J]. 光学学报, 2009, 29(9): 2552-2556.
- [23] Zhao Y Z, Sun H Y, Song F H, et al. Propagation properties of oblique and off-axial Gaussian beams passing through cat-eye optical lens[J]. Acta Optica Sinica, 2009, 29(9): 2552-2556.

# Influence of Mechanical Deformation of Off-Axis Optical Path on Coupling Efficiency in 3D Micro-Vibration Measurement

Dong Hui<sup>1</sup>, Wang Dayong<sup>2</sup>, Kong Xinxin<sup>3</sup>, Wang Yunxin<sup>2\*</sup>

<sup>1</sup>Faculty of Materials and Manufacturing, Beijing University of Technology, Beijing 100124, China;

<sup>2</sup>Faculty of Science, Beijing University of Technology, Beijing 100124, China;

<sup>3</sup>Key Laboratory of Computational Optical Imaging Technology, Chinese Academy of Sciences, Beijing 100094, China

## Abstract

**Objective** Three-dimensional (3D) laser Doppler micro-vibration measurement technology is widely applied in the research on dynamic characteristics of microstructures. Its two off-axis optical paths are employed to receive signal light containing in-plane vibration information. The optical fiber coupling efficiency in optical paths will directly affect the vibration measurement accuracy of the system. At present, the factors affecting the coupling efficiency of optical fiber mainly include optical system aberration, atmospheric turbulence, amplitude distribution type of signal light and local light, and optical system parameters. The effect of gravity, temperature, or mechanical deformation of optical elements during installation on the coupling efficiency is not considered. In addition, most of the current research focuses on one-dimensional laser Doppler detection system, and there is a lack of research on 3D laser Doppler micro-vibration measurement system, especially the off-axis optical path. To this end, based on the diffraction propagation theory and the fiber coupling principle, the optical transmission and coupling model of the off-axis signal receiving optical path in the 3D micro-vibration measurement system is built in this paper. The mechanical deformation of typical optical components in the system is analyzed, and the influence of these mechanical deformations on the fiber coupling efficiency is studied. In addition, the maximum tolerances of different mechanical deformations are given. The research is of guiding significance for the design and installation of 3D laser Doppler micro-vibration measurement system.

**Methods** The detection optical path of the 3D micro-vibration measurement system includes the main axis optical path and off-axis optical path. The main axis optical path is overlapped with the  $z$  axis. Its function is to incident the laser onto the object to be measured and receive the reflected signal light containing the vibration component information of the object in the  $z$  direction. The two off-axis optical paths are in the  $y-z$  plane and the  $x-z$  plane respectively, and the angle between them and the main axis optical path is  $40^\circ$ . They are employed to receive the reflected signal light containing the information of the vibration component of the object in the  $x$  and  $y$  directions. The object plane is inclined to the off-axis coupling lens plane, so the diffraction propagation between the two inclined planes needs to be considered. In this paper, the optical transmission model of the off-axis signal is built. Firstly, the optical field of the original object plane signal is projected onto the reference plane parallel to the coupling lens plane by the frequency domain coordinate rotation transformation method. Secondly, the optical field distribution of the reference surface is propagated to the coupling lens plane through diffraction, and then to the fiber plane through the phase modulation of the coupling lens. Subsequently, the optical field distribution on the fiber plane can be obtained. Finally, the ideal fiber coupling efficiency can be calculated by the mode field matching method combined with the mode field distribution of single-mode fiber. The relationship between different mechanical deformations and the coupling efficiency of optical fiber is obtained by analyzing the change of parameters in the coupling model of off-axis signal caused by different mechanical deformations.

**Results and Discussions** The relationship between mechanical deformation and fiber coupling efficiency is obtained by the coupling model of off-axis signal optical transmission. Firstly, the relationship between the eccentricity of the coupling lens and the coupling efficiency is studied (Fig. 4). When the coupling efficiency is better than 40%, the maximum allowable range of the offset is about  $\pm 1.5 \mu\text{m}$ . When the beam passes through the tilted coupling lens, the wavefront changes caused by the tilt of the lens near the front and rear surfaces cancel each other out. Therefore, the tilt of the coupling lens exerts no effect on the coupling efficiency if the aberration of the coupling lens is ignored. Next, the influence of the fiber misalignment and the fiber misalignment angle on fiber coupling efficiency is studied. The fiber coupling efficiency is more sensitive to the optical fiber misalignment in the  $x-y$  direction [Fig. 6(a)] and less sensitive to the optical fiber misalignment in the  $z$  direction [Fig. 6(b)], and the change with the optical fiber misalignment angle is less obvious (Fig. 8). In addition, the out-of-plane vibration caused by the object under test will also affect the fiber coupling efficiency of the off-axis optical path (Fig. 10). When the out-of-plane vibration displacement is within the range of  $\pm 3 \mu\text{m}$ , the coupling efficiency slowly decreases from 76.5% to about 60.0%, which is acceptable in the actual utilization of the

system.

**Conclusions** A coupling model of optical transmission and transmission of off-axis signals in a 3D laser Doppler micro-vibration measurement system is built. The effect of mechanical deformation on the optical coupling efficiency of off-axis signals in the system is further studied. The simulation results show that the off-axis optical coupling efficiency is sensitive to the coupling lens offset and the optical fiber misalignment. Under the micron displacement error, the off-axis coupling efficiency decreases sharply. Therefore, the two mechanical errors should be avoided first during the system design. The optical coupling efficiency of the off-axis signal is less sensitive to the defocus of fiber and the fiber misalignment angle. When the actual system is adopted, if the out-of-plane vibration range of the object to be measured is  $\pm 3 \mu\text{m}$ , the coupling efficiency of the off-axis signal light slowly decreases from 76.5% to about 60.0%, which has little influence on the system. When the aberration of the coupling lens is ignored, the coupling efficiency is not affected by the coupling lens tilt. This study is of guiding significance for the design of off-axis detection optical path of 3D laser Doppler micro-vibration measurement system. The diffraction propagation calculation and the construction and analysis of the coupling model can be further extended to other single-mode fiber imaging systems.

**Key words** measurement; interferometry; three-dimensional micro-vibration measurement; mechanical deformation; fiber coupling; diffraction propagation theory